Network-Independent Synchronous Stability Boundary and Spontaneous Synchronization

Yu Yuan *

Posted Date: 15 April 2025

doi: 10.20944/preprints202310.1791.v9

Keywords: stability boundary; synchronization; complex network

Article

Network-Independent Synchronous Stability Boundary and Spontaneous Synchronization

Yu Yuan

Sichuan Technology, China; yuyuan.sctbc@outlook.com

Abstract: Synchronization of complex networks has been widely studied. Current research on the synchronization of complex networks is based on concepts from graph theory and statistical physics. However, the study of real network synchronization remains present substantial obstacles. To overcome the difficulties caused by the complexity of the network, I report a simple synchronization stability boundary equation and identify a spontaneous synchronization structure in power grids for the first time. The findings indicate that both the synchronization stability boundary and the location of spontaneous synchronization occurred are independent of the network. The boundary equation harmonizes two contradictory conclusions well and reveals the mechanism of the synchronization of different individuals through coupling. These results offer a new direction for synchronization research, providing a means to overcome the challenges posed by network complexity, nonlinearity, and uncertainty, and enabling a unified approach to analyzing the synchronization stability of grids.

Keywords: stability boundary; synchronization; complex network

Introduction

The study of synchronization began with Huygens. As the number of studies on collective behavior in complex systems has grown, synchronization in coupled systems has garnered extensive attention [1]. Synchronization in complex systems [2], e.g., synchronous discharge, the flashing of fireflies, and the synchronization of generators, is widely observed in nature and industry.

It is widely believed that networks are closely related to spontaneous synchronization [2]. Current research on the synchronization of complex networks is based on concepts from graph theory and statistical physics, such as the connectivity of the graph and the nodal degree [2]. To analyze synchronization behaviors of complex networks, these approaches require clear information about the network structure and simplify the interactions between individuals into a coupled network. However, this is difficult to achieve in practice [3,4], as realistic interactions often cannot be observed. The complexity of real networks can also make topological information incomplete [5]. Additionally, overly large networks make clear topology modeling quite difficult. These challenges can lead to incorrect network reconfiguration and link predictions. Even if complete information regarding the network topology is obtained, other difficulties, such as the diversity of networks and community structures, uncertain dynamics and nonlinear network parameters, are often encountered simultaneously in real networks. These difficulties present substantial obstacles for the study of network synchronization.

To overcome the abovementioned difficulties, a network-independent synchronization analysis path is constructed for generator synchronization in power systems in this paper. Power systems are the largest man-made systems and are considered to be typical complex network systems. Therefore, the study of the synchronization behavior of generators in power grids is of critical importance not only for the stable operation of power systems but also for the wider field of synchronization of complex networks [1,2]. The approach in this paper identifies collective synchronization and those individuals not participating in it, based solely on the behavior of each individual in the system. In particular, this method reveals how individuals in the network are synchronized while ignoring the

network structure. This approach has been experimentally verified for the realistic power grid systems.

Synchronization is a prerequisite for the normal operation of a power grid [6]. Large power systems are complex coupled systems where nonlinearities and uncertainties coexist [7]. To analyze the synchronization of generators, numerous insightful methods are being developed [1,8–12], including the determination of synchronous stability boundaries [13–15] and the use of spontaneous synchronization conditions [2].

The identification of the synchronous stability boundary of a system is a key unresolved problem [14,16,17]. A stablity boundary is the union of critical points [18], and when the system state is outside the stability boundary, it is desynchronized [15]. The boundary, which is a core concept of grid stability, is closely related to many other issues encountered in power systems [19–21]. Therefore, investigations of synchronous stability boundaries can make a significant impact on the development of power systems and the synchronization stability of complex networks. The derivation of an analytical equation that can describe a boundary has been a long-standing research goal in the field of power systems [13,14,22]. However, current research is still limited by the nonlinearity and uncertainty of power systems. On the other hand, the spontaneous synchronization of complex systems has been utilized to elucidate the synchronized operation of generators in interconnected grids [23]. Therefore, many studies on power system stability are based on the knowledge of synchronization conditions of complex networks [2,23,24]. However, this scheme is in some cases considered to oversimplify real systems [9,23], and it has been argued that self-organization is not relevant for a power grid [9].

Here, an equation is derived and visualized based on a succinct consensus. The equation describes the synchronous stability boundary of a power system in a unified manner and has elegant formal and physical interpretations. I started by showing the validity of the boundary equation with three pieces of evidences. These evidences demonstrate that this approach addresses the problems of the multiswing stability discrimination of multiple generators in a power system and partial synchronization. Subsequently, I demonstrated that the synchronous stability boundary is independent of the network structure and parameters. It is also shown here that the synchronization stability of the power system is determined by the amplitude, while the conclusion that both symmetry and asymmetry promote synchronization is discussed. In addition, by comparing the boundary with the location of synchronization occurred, I observed that spontaneous synchronization occurs only close to the boundary and is manifested as a specific structure. This represents the first clear evidence of spontaneous synchronization in a power system. Moreover, this close connection suggests that, like the synchronous stability boundary, the spontaneous synchronization on a network is also not directly related to the network. This novel approach is developed to investigate the synchronization of complex networks, taking into account potential scenarios of realistic network complexity, nonlinearity, or uncertainty. The conclusion in this paper may inspire advances in other disciplines.

Stability Boundary

Synchronization occurs when the coupling dominates the dissimilarity [2]. Currently [2], the coupling is typically quantified by graph theory, and the dissimilarity is quantified by the frequencies ω_i. In this work, it is assumed that the coupling is quantified by the coupling power and the dissimilarity is quantified by the dissimilar power. When the generators are synchronized, there is no dissimilarity, meaning the dissimilar power is 0. The coupling power is denoted as $P_{\Delta u}$ and the dissimilar power is denoted as $P_{\partial u}$. That is, when $P_{\Delta u} \geq P_{\partial u}$, the system is synchronous and stable, otherwise it is out of synchronization. Therefore, $P_{\Delta u} = P_{\partial u}$ represents the synchronous stability boundary. This assumption quantifies the interactions between individuals and is not based on graph theory or statistical physics concepts.

The boundary equation is expressed as follows:

$$\left(|u_K| = |u_L|\right) \cup \left(\frac{|u_L|}{|u_K|} = 2\cos\delta_{K,L} - 1\right) \quad (1)$$

where $|u_K| > |u_L| \geq 0, |\delta_{K,L}| \geq 0$. Eq. (1) is the specific expression of $P_{\Delta u} = P_{\partial u}$ in the power system.

Here, u_K, u_L denote the voltages per unit of the Kth and Lth meta-generators, respectively. The meta-generators are "the map of the generators" (refer to Eq. S2). The voltage has been previously overlooked for simplicity [9,23] but is crucial for the synchronization stability of the grid. ω_i is the rotor speed per unit of the ith meta-generator, which is a normalization quantity commonly used in power system studies. $\delta_K = 2\arctan(\omega_K)$ is defined as the angle of rotation rate of the Kth meta-generator. The angle difference of rotation rate between the Kth and Lth meta-generators is $\delta_{K,L} = |\delta_K - \delta_L| \geq 0$. It is important to note that δ_K is not a phase and that $L = K + 1$. According to the definition of synchronization, $\delta_1 = \cdots = \delta_K = \delta_L = \cdots = \delta_n$.

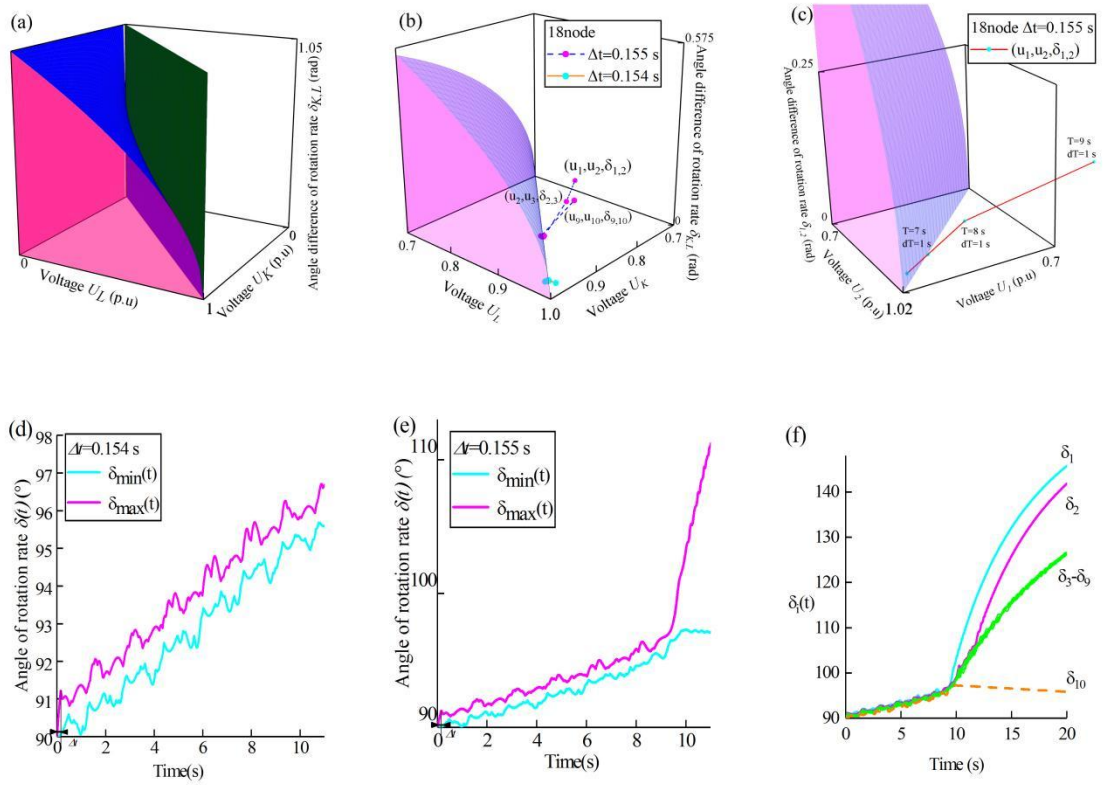

Figure 1. Stability boundary. A New England test system (10-gen) was used. A three-phase short-circuit ground fault occurred at node 18.

(a). Visualization of the stability boundary. The stability boundary in Eq. (1) (blue surface and dark green plane) and the pink planes $0 - u_L - \delta_{K,L}$, $u_K - 0 - \delta_{K,L}$ and $u_K - u_L - 0$ collectively define the boundaries and enclose the stability domain.

(b). The boundary distinguishing synchronization stability. The dark green plane is not shown. Δt is the fault clearing time. $(u_K, u_L, \delta_{K,L})$ is defined as the coordinate of the coupling point of the Kth and Lth meta-generators, and it is computed from u_K, δ_K, u_L and δ_L.

$d(\Delta t) = 0.155\ s - 0.154\ s = 0.001\ s$ denotes the step length commonly used in power system studies. The coupling points in panel (b) are calculated using Eqs. (S3) and (S4).

(c). The boundary and the stability of multiple swings for multiple generators. For clarity, part of the disturbed trajectory of $(u_1, u_2, \delta_{1,2})$ is selected. Each cyan point represents the mean position of $(u_1, u_2, \delta_{1,2})$ for a period of 1 second ($\Delta t = 0.155\ s$). The time T=8 s and the time interval $dT = 1s$ are defined in Eq. (S5). The plane $|u_L| = |u_K|$ is not shown here.

(d) and (e). The results of the numerical experiment at $\Delta t = 0.154s$ and $\Delta t = 0.155\ s$. The horizontal axis represents the time. The maximum value of $\delta_i(t)$ is represented by the magenta curve, and the minimum value is represented by the cyan curve. $\delta_{\min}(t) \le \delta_i(t) \le \delta_{\max}(t)$. At 11 second, $\delta_{\max}(t) - \delta_{\min}(t) \approx 1°$ in (d), and $\delta_{\max}(t) - \delta_{\min}(t) \approx 14°$ in (e). As illustrated in panel (d), the $\delta_i(t)$ values of all meta-generators are close to each other and have approximately the same rate of change. panel (e) shows that in the time interval $(9\ s, 10\ s)$, $\delta_{\max}(t) - \delta_{\min}(t)$ increases sharply, indicating generator desynchronization.

(f). The phenomenon of partial synchronization and the stability of multiple swings for multiple generators. $\Delta t = 0.155\ s$. After approximately 9 seconds, meta-generator 1 disengages from the cluster (cyan line). Subsequently, meta-generators 10 (magenta line) and 2 (orange dashed line) are separated. Meta-generators 3~9 form a synchronized cluster (green lines). $\delta_i(t)$ in panels (d), (e) and (f) are calculated using simulation software and Eq. (S2).

Three pieces of evidence demonstrate that Eq. (1) effectively describes the synchronization stability boundary: 1) the boundary effectively distinguishes between stable and unstable states of the power system [see Figs. 1(b) and S1(a)], 2) the stability of multiple swings [see Figs. 1(c) and S1(b)], and 3) the partial synchronization phenomenon [see Figs. 1(f) and S1(e)].

Figure 1(b) illustrates that the synchronization stability boundary effectively differentiates between synchronized and desynchronized states.. A system comprising n meta-generators possesses n-1 coupling points. The behavior of the cyan and magenta dots is significantly different, despite the slight difference in Δt (Fig. 1(b)). When $\Delta t = 0.154\ s$, all of the cyan coupling points are clustered at the boundary. When $\Delta t = 0.155\ s$, the three magenta coupling points, i.e., $(u_1, u_2, \delta_{1,2})$, $(u_2, u_3, \delta_{2,3})$, and $(u_9, u_{10}, \delta_{9,10})$, are outside the boundary and away from the rest of points. As mentioned above, when $P_{\Delta u} < P_{\partial u}$, the coupling point $(u_K, u_L, \delta_{K,L})$ is outside the boundary and the power system is out of synchronization. Consequently, it is concluded that the system is stable at $\Delta t = 0.154\ s$ and out of synchronization at $\Delta t = 0.155s$. The results in Figs. 1(d) and (e) are in good agreement with this conclusion. Additional analogous results can be found in Fig. S8.

Furthermore, utilizing Fig. 1(b) facilitates easily identify different synchronization patterns as it provides specific information about synchronized and desynchronized individual meta-generators or groups of meta-generators. The New England test system comprises 10 meta-generators, which is equivalent to 9 coupling points. As shown in Fig. 1(b), the 3 coupling points $(u_1, u_2, \delta_{1,2})$, $(u_2, u_3, \delta_{2,3})$ and $(u_9, u_{10}, \delta_{9,10})$ are outside the boundary while the rest of the points are clustered near the boundary. This signify that the meta-generators are divided into 4 synchronization groups. Specifically, $(u_1, u_2, \delta_{1,2})$ outside the boundary means that the meta-generators 1 and 2 are not synchronized. There are analogous conclusions for $(u_2, u_3, \delta_{2,3})$ and $(u_9, u_{10}, \delta_{9,10})$. That is, the meta-generators numbered 1, 2 and 10 are out of synchronization while the other meta-generators

remain synchronized. This indicates that the meta-generators in each group are also clearly shown in Fig. 1(b). The result for the meta-generator synchronization group shown in Fig. 1(f) is in good agreement with those presented in Fig. 1(b). This is the phenomenon of partial synchronization. These results suggest that the partial synchronization phenomenon [25–28] is caused by the loss of synchronization stability among these individuals or groups. This interpretation will deepen our understanding of the complex phenomenon of partial synchronization.

Figure 1(c) clearly shows the transition of the power system from stabilization to instability. As shown in Fig. 1(c), $\left(u_1, u_2, \delta_{1,2}\right)$ crosses the boundary outwardly during the time interval $(8s,9s)$. Subsequently, $\delta_{1,2}$ increases dramatically during the time interval $\left(9\,s, 10\,s\right)$. These results are in good agreement with the simulation result presented in Fig. 1(e). The simulation result demonstrates that the system loses synchronization during the aforementioned time interval. Therefore, the time at which the coupling point crosses the boundary is the onset of synchronization loss. These results pertain to the stability of multiple swings for multiple generators, an important issue that has not been resolved to date [29,30]. The above results demonstrate the synchronization stability boundary expressed by Eq.(1) can discriminate the stability of multiple swings for multiple generators in real time. More importantly, this finding suggests that the synchronous stability boundary and the multimachine multiswing stability boundary are, in fact, identical. This result helps analyze the synchronous stability of the power system in a unified way.

The numerical experimental results in Figs. 1(d), (e) and (f) are time-series data independently calculated by the simulation software. The results in Figs. 1(b) and (c) are in good agreement with these experimental data. The above results provide solid evidences for the correctness and validity of the boundary equation from various perspectives.

As shown in Fig. 1(a), geometrically, Eq. (1) represents two surfaces in a coordinate system $u_K - u_L - \delta_{K,L}$. The left-hand side of Eq. (1) corresponds to a plane (dark green) perpendicular to the plane $u_K - u_L$, and the right-hand side corresponds to a curve surface (blue). These two surfaces are clearly fixed, i.e., they are independent of network topology and parameters. Therefore, Eq. (1) is independent of the network topology, system parameters, perturbations and number of subsystems. This finding, which contradicts previous reports [2,13,14], indicates that the stability boundary is independent of these factors. I emphasized that $\frac{|P_{\partial u}|}{|P_{\Delta u}|}=1$, not $P_{\Delta u}$ and $P_{\partial u}$, is independent of the network topology. The impact of the network is nullified through division (refer to "Derivation of the boundary equation").

The most straightforward **method** to prove that "the boundary is independent of the network" is to test whether Eq. (1) holds true for a completely different network. Analogous results were obtained for the 3-generator test system using the same procedure (see Fig. S1). Fig. 1 shows the results of the simulation with the New England test system, whereas the results in Fig. S1 are from the 3-generator test system. The New England test system and 3-gen are two completely different network systems. They clearly have completely different topologies and parameters, but in both cases, the same boundary equation is applied. This is because the aforementioned evidence can be reproduced in the 3-generator test system. Both Fig. S1(a) and Fig. 1(b) correspond to evidence 1) mentioned above. Both Fig. S1(b) and Fig. 1(c) correspond to evidence 2). Both Fig. S1(e) and Fig. 1(f) correspond to evidence 3). Consequently, a comparison of Figs. 1 and S1 reveals that Eq. (1) can be used to characterize the boundary of a different network. Moreover, the failures occurring on different network nodes can lead to different network structures. That is, the results in Fig. S8 can be considered as coming from different networks. These results also show that Eq. (1) is independent of the network. Eq. (1) is the analytical equation for the synchronous stability boundary. Therefore, these findings demonstrate that the synchronization stability boundary is independent of the network structure and parameters. This conclusion is at least applicable to those reconfigurable networks.

Eq.(1) can be a good solution for multiple generators' synchronization stability, the stability of multiple swings for multiple generators, and partial synchronization.

More information can be obtained from the expression of Eq. (1). Specifically, the left-hand side of Eq. (1) represents the global stability domain [13] (i.e.,when $|u_L|=|u_K|$, $\forall \delta_{K,L} \geq 0, P_{\Delta u} = P_{\partial u}$). $|u_L|=|u_K|$ is a manifestation of the symmetry of the system. This finding shows that high symmetry can promote synchronization in complex networks. This can explain why symmetric networks have better synchronization capabilities. This has been reported in various studies [31,32].

The right-hand side of Eq. (1) has a variant that is expressed by:

$$\delta_{K,L}^{cr} = \arccos(1-\frac{|u_K|-|u_L|}{2|u_K|}) \quad (2)$$

where $\delta_{K,L}^{cr}$ is the stability margin of the Kth and Lth meta-generator angle difference of the rotation rate. That is, for $(u_K, u_L, \delta_{K,L})$, the system remains synchronously stable when $\delta_{K,L}^{cr} > \delta_{K,L}$. The difference between $|u_K|$ and $|u_L|$ can be used to measure the degree of asymmetry of the system. Clearly, when $|u_K|, |u_L|$ are sufficiently close [32], $\delta_{K,L}^{cr}$ tends to 0. As $|u_K|-|u_L|$ increases, $\delta_{K,L}^{cr}$ increases. In other words, the synchronization stability domain becomes larger as the degree of asymmetry increases. This explains the recently discovered superior synchronization stability of highly asymmetric systems [6,33]. It is very difficult to maintain a high degree of symmetry at all times after the system is perturbed. For those systems requiring stability, asymmetry may be a more economical candidate. When $\delta_{K,L}^{cr} > \frac{\pi}{3}$, the Kth and Lth meta-generators are not synchronized.

Consequently, both high symmetry and high asymmetry promote synchronization. The expression of Eq. (1) is very simple, yet it *harmonize*s these two contradictory conclusions well and requires no additional assumptions.

In summary, Eq. (1) enables a unified analysis of the synchronization stability of the grid and provides a new understanding of synchronization. To determine the stability of a power system of n generators, only n pairs of variables $u_i, \delta_i, i \in (1,2,...,n)$ are required. These variables are physically meaningful and can be readily obtained. This greatly simplifies the study of grid synchronization stability.

Currently, for unknown complex networks, it is necessary to reconstruct the network structure based on the time series data of the system state before analyzing synchronization. The approach in this paper links these states directly to the synchronization analysis and the expression for the synchronization stability boundary is so simple.

Spontaneous Synchronization

Synchronized systems may be destabilized when they are disturbed. Therefore, it is equally important to study the the transition behavior of a disturbed system from stable to unstable states. I have observed that when the system is disturbed and on the brink of destabilization, the trajectory of the operating point becomes intriguing. A surprisingly specific structure emerges from the collective behavior of these trajectories. The operating point of the ith meta-generator is denoted by (u_i, δ_i).

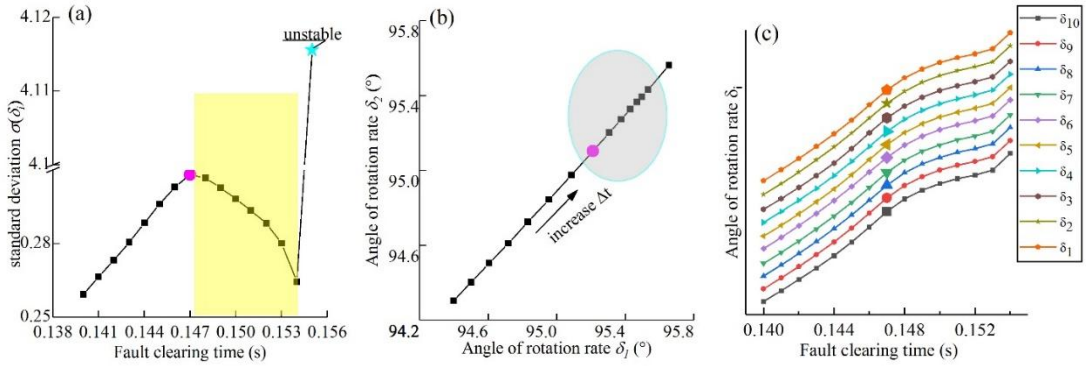

Figure 2. Spontaneous synchronization and unique structure. The fault clearing time Δt increases from 0.140 s to 0.155 s. The arrow means the direction of increase in Δt (the 18-node three-phase short circuit to the ground fault). $d(\Delta t) = 0.001\,s$.

(a). Spontaneous synchronization of meta-generators. The horizontal axis represents the fault clearing time. The vertical axis represents the standard deviation of δ. The yellow area means the thin layer where spontaneous synchronization occurs. Here, $\sigma(\delta_i)$ denotes the standard deviation of δ, which begins to decrease at 0.147 s (magenta dots) and increases by 1300% at 0.155 s when the system becomes unstable (cyan pentagram dots). $\sigma(\delta_i)$ can be calculated using Eq. (S6).

(b). The phenomenon of potential barrier on plane $\delta_1 - \delta_2$. Δt increased from 0.140 s to 0.154 s. The black arrow means the direction in which Δt increased. From $\Delta t = 0.147\ s$ (the magenta dot) onward, the distance between neighboring points decreased in the direction of the black arrow (the elliptical shaded area).

(c). Starting points of spontaneous synchronization and long-range correlation. The horizontal axis represents the fault clearing time. The amplified points mean the starting points of spontaneous synchronization. Near the boundary, all of starting points appear at $\Delta t = 0.147\ s$. The disturbance trajectories of all of the points were almost identical. δ_i in panels (b) and (c) are calculated using Eq. (S3)..

As shown in Fig. 2(a), $\sigma(\delta_i)$ exhibits discontinuity at 0.154 s and 0.155 s. In agreement with the findings presented in Fig. 1, the system is stable at $\Delta t = 0.154\,s$ and unstable at $\Delta t = 0.155\,s$. The decrease in $\sigma(\delta_i)$ from the highest point in the yellow region indicated that on the brink of destabilization, the velocity of the subsystem was spontaneously directed toward the mean value. This counterintuitive phenomenon is consistent with the definition of spontaneous synchronization effect [8,35]. The spontaneous synchronization effect causes $\sigma(\delta_i)$ to decrease whether the operating point crosses the potential barrier in the inward or outward direction. Therefore, within the thin layer, the results of $\sigma(\delta_i)$ in different directions are not the same. This may form a hysteresis loop of $\sigma(\delta_i)$ in these directions.

Although spontaneous synchronization has been utilized to understand the synchronous operation of generators [23], certain studies have cast doubt on the existence of spontaneous synchronization in power systems [9]. The reason for these doubts is that current research has not uncovered direct evidence of self-organizing synchronization in the power system, nor has it shown exactly where it occurs. Self-organizing behavior emerges from the interactions of these meta-generators, and its effects are reflected in the perturbation trajectories at the operating point. As shown in Fig. 2(b), for a constant step size $d(\Delta t) = 0.001\,s$, the interval between points decreases

progressively within the shaded area, leading to the emergence of a unique trajectory structure. I refer to this novel structure as a "potential barrier" because the points within the shaded area exhibit "decelerating motion", as if the mass points were crossing a potential barrier. To the best of my knowledge, this structure has not been previously reported. $\sigma(\delta_i)$ reaches its maximum at $\Delta t = 0.147\ s$ and begins to decrease in Fig. 2(a). The magenta dot corresponds exactly to $\Delta t = 0.147\ s$ in Figs. 2(b). All of amplified points appear at the identical Δt in Fig. 2(c). These amplified points are located at the transition of $\frac{d^2\delta_i}{d(\Delta t)^2}$. Prior to this, $\frac{d^2\delta_i}{d(\Delta t)^2} > 0$. After this, $\frac{d^2\delta_i}{d(\Delta t)^2} < 0$. Moreover, the system is unstable at $\Delta t = 0.155\ s$. These results demonstrate that $\Delta t = 0.147\ s$ is the starting point and $\Delta t = 0.154\ s$ is the end of spontaneous synchronization. This is the position of spontaneous synchronization where emergence occurs.

Currently, spontaneous synchronization is considered to be closely related to the network structure [36]. However, the results of this paper yield another conclusion. I want to emphasize that the "spontaneous synchronization" in this paper refers only to the position of spontaneous synchronization where emergence occurs. The experimental results show that the thin layer where spontaneous synchronization occurred is found only close to the synchronization stability boundary. Different failures led to different network structures. Similar to Fig. 2(a), those results in Fig. S5 from different network structures suggest that a decrease in $\sigma(\delta_i)$ occurs only when the system is on the brink of lose synchronization. In other words, the system suddenly self-organizes toward synchronous evolution only when it about to reach a critical synchronous stable state. Additionally, a comparison of Figs. 2(a) and S2(a) indicates that the same conclusion holds true for a completely different network. These phenomenon can be interpreted as spontaneous synchronization occurring only close to the synchronous stability boundary. Eq. (1) describes the stability boundary of the power system. Consequently, for coupled network systems, the link between spontaneous synchronization and the boundary suggests that the location where spontaneous synchronization occurs is constrained by Eq. (1). As mentioned above, Eq. (1) is independent of the network. This finding suggests that spontaneous synchronization is independent of the network. This conclusion challenges the traditional perception of spontaneous synchronization in networks.

Additionally, when $P_{\Delta u} = P_{\partial u}$, collective synchronization emerges from individuals' behavior. Specifically, at $\Delta t = 0.147\ s$, $\frac{d^2\delta_i}{d(\Delta t)^2}$ of all meta-generators transforms simultaneously (refer to Fig. 2(c)). Given that these meta-generators are connected to different nodes, this result suggests that they exhibit long-range correlation at the point of impending destabilization. This correlation leads to a collective movement of all individuals as a whole.

Current research on synchronization phenomena focuses on the transition from disorder to synchronization. There are few references to "the emergence of spontaneous synchronization during the evolution of a fully synchronized system to disorder". The paper shows that the system also undergoes self-organization before it loses synchronization stability. Synchronization emerges from disorder when an operating point crosses the boundary in the inward direction. In this case, spontaneous synchronization may have different initial values and conditions, and it is not clear where it is started, which is an important issue that is not discussed in this paper. Considering that u_i changes before δ_i and that $P_{\Delta u} = P_{\partial u}$ is a phase transition point, I infer that the boundary is the onset of synchronization in that case.

The behavior of the operating point near the boundary is diverse. For example, A comparison of Figs. 2 and S2 reveals that spontaneous synchronization can result in at least two different results.

The reasons for this difference, or rather, the specific conditions for the formation of a potential barrier, require further research. Moreover, the thin layer where spontaneous synchronization occurs has some thickness. This thickness may be related to the network topology and parameters, but its solution is not clear. These issues will be addressed in future research.

Materials and Methods

There is a consensus in the literature: Synchronization occurs when the coupling dominates the dissimilarity [2]. Currently, the coupling is typically quantified by graph theory, and the dissimilarity is quantified by the frequencies ω_i.

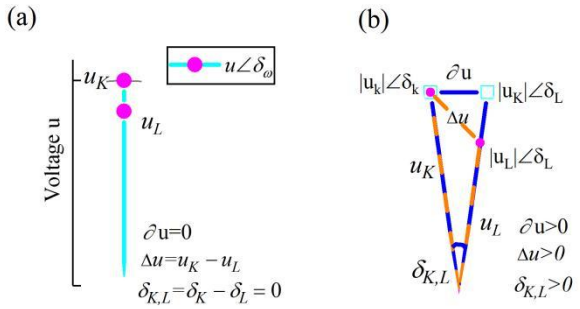

Figure 3. Schematic diagram. Fig. 3 is an analogous illustration of the amplitude angle $U_i\angle\delta_i$ which is the foundation of power system analysis.

(a). The generators are kept in synchronized operation. The magenta dot indicates the ith generator $u_i\angle\delta_i$. The length of the solid cyan line represents the generator port bus voltage amplitude $|u_i|$. The angle of the solid line $\delta_i = 2\arctan(\omega_i), i=1,2,\cdots,n$ is defined as the angle of rotation rate of the Kth meta-generator. Note that δ_i is not a phase. ω_i is the rotor speed per unit of the Kth meta-generator. Specifically, for the power system, when the generator operates synchronously, $\omega_1=\omega_2=\cdots=\omega_n=1$, and $\delta_i=\frac{\pi}{2}, i=1,2,\cdots,n$.

(b). Following a disturbance in the power system, $\omega_K\neq\omega_L$, and $\delta_{K,L}>0$. Δu is defined as "the coupling potential difference" between the Kth and Lth meta-generators (the orange dotted line between the magenta square dots). Correspondingly, ∂u is constructed to describe "the dissimilar potential difference" between the Kth and Lth meta-generators (the solid blue line between the cyan dots).

In real operating power systems, the generator port bus voltages (per unit value) u_K and u_L are often unequal. That is, when all generators operate synchronously, the coupling strength between them is greater than 0 because of the difference between u_K and u_L (i.e., $\delta_{K,L}=0, \Delta u=u_K-u_L>0$)[see Fig. 3(a)]. Unlike in the previous method, the coupling strength between the nodes is quantified by $P_{\Delta u}$. $P_{\Delta u}$ is the coupling power. $P_{\Delta u}>0$.

On the other hand, the dissimilarity between the nodes is quantified by $P_{\partial u}$. $P_{\partial u}$ is named the dissimilar power. $P_{\partial u}=0$ corresponds to complete synchronization. When all the generators are completely synchronized(i.e., no dissimilarity), $P_{\partial u}=0$ (i.e., $\delta_{K,L}=0, \partial u=0$). Following a

disturbance in the power system, the generators' rotational speeds are dissimilar, $P_{\partial u} > 0$ (i.e., $\delta_{K,L} > 0, \Delta u > 0, \partial u > 0$) [see Fig. 3(b)].

The expressions for $P_{\Delta u} = \frac{|\Delta u|^2}{|Z_{K,L}|}$ and $P_{\partial u} = \frac{|\partial u|^2}{|Z_{K,L}|}$ are analogous to those of $P_{K,L} = \frac{|\vec{U}_K - \vec{U}_L|^2}{|Z_{K,L}|}$, which can represent the interaction between the nodes in a power system. $P_{\Delta u}$ and $P_{\partial u}$ have the same dimension and can be directly compared in size. $Z_{K,L}$ is the impedance between the Kth and Lth meta-generators.

Considering the consensus mentioned earlier, the boundary equation is expressed as $P_{\Delta u} = P_{\partial u}$ in the grid. When $|P_{\partial u}| \le |P_{\Delta u}|$, the system is synchronous and stable. Conversely, when $|P_{\partial u}| > |P_{\Delta u}|$ [to fulfill this condition, $\partial u(u_K)$ is chosen instead of $\partial u(u_L)$ in Eq. (S1)], the system is out of synchronization and unstable.

I emphasize that $\frac{|P_{\partial u}|}{|P_{\Delta u}|} = 1$, not $P_{\Delta u}$ and $P_{\partial u}$, is independent of the network topology. It is clear from the form of $P_{\Delta u}$ and $P_{\partial u}$ that they are related to the network, as information about the network is contained in $Z_{K,L}$. However, $\frac{|P_{\partial u}|}{|P_{\Delta u}|} = 1$ eliminates $Z_{K,L}$. It is observed that $\frac{|P_{\partial u}|}{|P_{\Delta u}|} = 1 \Leftrightarrow \frac{|\partial u|}{|\Delta u|} = 1$. The set of points for which $|\partial u| = |\Delta u|$ is the synchronous stability boundary.

As shown in Fig. 3(b),

$$\Delta u = \sqrt{u_K^2 + u_L^2 - 2u_K u_L \cos\delta_{K,L}},$$
$$\partial u = \sqrt{2u_K^2(1-\cos\delta_{K,L})}. \quad \text{(S1)}$$

The symbols "Δ" and "∂" are for distinction only and have no mathematical significance. Thus, Eq. (1) is obtained via derivation from $u_K^2 + u_L^2 - 2u_K u_L \cos\delta_{K,L} = 2u_K^2(1-\cos\delta_{K,L})$. Clearly, the only variables in Eq. (1) are u_K, u_L and $\delta_{K,L}$.

$f\left(u_K, u_L, \delta_{K,L}\right) = \frac{|\partial u|}{|\Delta u|} = 1$ is the stability boundary equation. When $\frac{|\partial u|}{|\Delta u|} < 1$, the system is stable. When $\frac{|\partial u|}{|\Delta u|} > 1$, the system is unstable. Geometrically, $f\left(u_K, u_L, \delta_{K,L}\right) = 1$ describes exactly curved surfaces that, together with $(0, u_L, \delta_{K,L})$, $(u_K, 0, \delta_{K,L})$ and $(u_K, u_L, 0)$ encloses a stable domain.

In summary, the boundary equation $|u_K| = |u_L| \cup \frac{|u_L|}{|u_K|} = 2\cos\delta_{K,L} - 1$ can be found, where $|u_K| \ge |u_L| \ge 0, |\delta_{K,L}| \ge 0$. The coordinate system $u_K - u_L - \delta_{K,L}$ is established, and the boundary is visualized (Fig. 1(a)).

Power Grid Datasets

Here, I describe the sources of data for the two power-grid networks considered in this study, namely the 3-generator (3-gen) test system and the New England (10-gen) test system [31,32]. The results of utilizing the New England test system are shown in Figs. 1, 2, S3, S4, S5, S6, S7, and S8, and the results of utilizing the 3-generator test system are shown in Figs. S1 and S2.

For each system, the data provide the generators' dynamic parameters, the net injected real power at all generator nodes, the power demand at all nongenerator nodes, and the parameters of all power lines and transformers. These parameters are sufficient for standard power flow calculations and stability calculations [6].

WECC 3-generator test system (3-gen). This system represents the Western System Coordinating Council (WSCC), which is part of the region now called the Western Electricity Coordinating Council (WECC) in the North American power grid. All the parameters mentioned above are from ref. 31.

New England test system (10-gen). The IEEE 39 bus system is well known as the 10-machine New England Power System. Generator 1 represents the aggregation of many generators. All the parameters mentioned above are from ref. 32.

The significance of using two entirely distinct test systems is much greater than that of merely adding a few numerical results. More crucially, this serves to demonstrate the applicability of the assumption of this paper to a completely different network.

Simulation Software

In principle, the swing equation can be used to analyze the synchronization of the generators. The expression of this equation is

$$\begin{aligned} \frac{d\theta_i}{dt} &= \omega_i \\ I_i \frac{d\omega_i}{dt} &= P_i - \gamma_i \omega_i + \sum_{j=1}^{N} K_{ij} \sin(\theta_j - \theta_i) \end{aligned} .$$

where γ_i is the damping of an oscillator, I_i is the inertia constant and K_{ij} is a coupling matrix governing the topology of the power grid network, and the strength of the interactions. θ_i is the voltage phase angle. However, it is considered for application to short-term dynamics (of the order of one second or less) in power systems [see Ref. 6]. Therefore, each of the two models was simulated separately in this paper via the Power System Analysis Software Package (PSASP), a simulation software. The PSASP has built-in more accurate and improved oscillation equations that are not limited by short-term dynamics. The software can be used to compute time series data for the rotation rate and voltage. I utilized the software to perform standard power flow calculations on two test systems and to calculate the dynamic parameters of generators after a three-phase short-circuit ground fault, respectively.

The standard power flow calculation calculates the voltage, current and other physical quantities of the power system in steady-state operation. For the PSASP, the power flow calculation is the basis of the stability calculation. The mathematical model for stability calculation includes the mathematical description of the power grid and the dynamic characteristics of the equipment, as well as the simulation of various possible disturbance modes and stabilization measures. The techniques for power flow calculation and stability calculation are well established. For detailed knowledge on power flow calculations and stability calculations, see related textbooks or Refs. 11, 29. Notably, Eq. (1) is not the result of a power flow calculation or stability calculation.

Experimental Steps and Data Processing

The selection of parameters should adhere to the following principles: 1) The coupling strength and the dissimilarity can be quantified and constructed as an expression of the energy function by the selected parameters. 2) When the subsystems are coupled but not dissimilar, $P_{\Delta u} > 0$ and $P_{\partial u} = 0$. 3) The number of parameters should be sufficiently small to prevent dimensional catastrophe. 4) The selected parameters should have a clear physical meaning and be easily accessible. Consequently, careful selection of suitable parameters is essential. For power systems, u_i and ω_i are suitable parameters. In real systems, these parameters can be measured directly. I calculate the rotation rate and voltage of the generator via the aforementioned simulation software.

First, I model the networks of the test systems in the software package and input the data. I utilized the standard power flow calculation program to obtain data such as the port bus voltage of the generator. For steady state operation, the frequency base value is set at 50 Hz.

To observe the response of the disturbed operating point, I turned off the controls. Prior to performing stability calculations, I fixed the fault location (e.g., node 18 in the New England test system, as shown in Figs. 1 and 2) and specified the fault type and the fault clearing time Δt. All fault types discussed in this paper were set as a three-phase short circuit to ground. I calculated the rotation rate $\omega_i'(t)$ and port bus voltage $u_i'(t)$ of the ith generator for various fault clearing times Δt. To test the effectiveness of the approach for the stability of multiple swings, the time window T was set to 20 seconds. That is, using the start of the disturbance as a starting point, I calculated and recorded the generator data for the next 20 seconds. The fault location and type remain unchanged, a new fault clearing time $\Delta t + d(\Delta t)$ was set, and the above steps were repeated until the system loses synchronization stability (Figs. 1(e) and S1(d)). $d(\Delta t)$ denotes the step length.

The angle of rotation rate of the ith generator was subsequently calculated as $\delta_i'(t) = 2\arctan[\omega_i'(t)]$. The extensive interconnections between generators make stability analysis very challenging (see Fig. S3). This challenge arises from the complexity of the network. In order to analyze the phenomenon of partial synchronization and to reduce the dimensionality, the concept of a meta-generator is introduced here. At moment t, the instantaneous values of the n generator system $\left(u_i'(t), \delta_i'(t)\right), i = 1, 2, \cdots, n$ are arranged in descending order by δ_ω, relabeled, and then reconstituted as the n meta-generator system $\left(u_i(t), \delta_i(t)\right), i = 1, 2, \cdots, n$.

In other words, when the condition $\delta_{i+1}'(t) > \delta_i'(t)$ holds,

$$\begin{aligned} (u_{i+1}(t), \delta_{i+1}(t)) &= (u_i'(t), \delta_i'(t)), \\ \left(u_i(t), \delta_i(t)\right) &= \left(u_{i+1}'(t), \delta_{i+1}'(t)\right). \end{aligned} \tag{S2}$$

A meta-generator is created by reordering and labeling generators. This is a technical treatment only, and this transformation has been shown not to change the pattern of change in the state of the system [see Figs. S4(a), S6 and S7]. In this way, I obtain the meta-generator data $\left(u_i(t), \delta_i(t)\right), i = 1, 2, \cdots, n$. Before and after the transformation, the numbers of generators and meta-generators are equal. Notably, Eq.(S2) may suggest that the coupling within the system may be influenced by some kind of "order pattern" defined by key parameters [refer to Fig. S3].

The operating point of the ith meta-generator is represented by (u_i, δ_i). The coupling point of the Kth and Lth meta-generators is represented by $(u_K, u_L, \delta_{K,L})$. These data can be utilized as coordinates for visualization, as shown in Fig. 1. These points are calculated as follows:

The means of $\left(u_i(t), \delta_i(t)\right), i = 1, 2, \cdots, n$ over $[0, T]$ were

$$u_i = \frac{1}{T}\int_0^T u_i(\tau)d\tau,$$
$$\delta_i = \frac{1}{T}\int_0^T \delta_i(\tau)d\tau \tag{S3}$$

and

$$\delta_{K,L} = \frac{1}{T}\int_0^T \delta_{K,L}(\tau)d\tau = \frac{1}{T}\int_0^T \left|\delta_K'(\tau) - \delta_L'(\tau)\right| d\tau$$
$$= \frac{1}{T}\int_0^T \delta_K(\tau) - \delta_L(\tau)d\tau = \delta_K - \delta_L. \tag{S4}$$

The results are shown in Figs. 1(b), 2(b), S2(a), etc.

After disturbance, the location of the coupling point varies with time. The means of $\left(u_i(t), \delta_i(t)\right), i = 1, 2, \cdots, n$ over $[T, T+dT]$ were

$$u_i(dT) = \frac{1}{dT}\int_T^{T+dT} u_i(\tau)d\tau,$$
$$\delta_{K,L}(dT) = \delta_K(dT) - \delta_L(dT) = \frac{1}{dT}\int_T^{T+dT} \left[\delta_K(\tau) - \delta_L(\tau)\right]d\tau, \tag{S5}$$

where dT is the time interval. The results are shown in Figs. 1(c) and S2(b).

Near the boundary, δ_i was calculated at a relatively fine scale. The standard deviation of δ_i is calculated as follows:

$$\sigma\left(\delta_i\right) = \sqrt{\frac{\sum_{i=1}^{n}\left(\delta_i - E\left(\delta_i\right)\right)^2}{n}},$$
$$E\left(\delta_i\right) = \frac{\sum_{i=1}^{n}\delta_i}{n}. \tag{S6}$$

where $E\left(\delta_i\right)$ is the expectation of δ_i. The results are shown in Figs. 2(a), S2(a) and S5.

Base Frequency and Proof of the Boundary Equation

Let $\delta_i = 2\arctan\frac{\omega_i}{\omega_0}$, where ω_0 represents the power system base frequency. Base values constitute fundamental concepts in power system analysis. For example, through voltage base values, a multilayer power network can be reduced to a single-layer equivalent, significantly simplifying network analysis. Similarly, the base frequency ω_0 plays a critical role in system stability analysis. ω_0 is constrained to positive real numbers. Typically, the equilibrium point corresponding to the synchronized state is selected as ω_0. For a power system in steady state operation, the base frequency generally coincides with the system's rated frequency (50 Hz or 60 Hz in most power grids globally). As previously stated in this paper, $\omega_0 = 50Hz$. Can ω_0 be eliminated from the boundary equation? i.e., is there a synchronization stability boundary based on individual behaviors for power systems that operate asynchronously?

When $\delta_i = 2\arctan\frac{\omega_i}{\omega_0}$ is substituted into Eq. (1),

$$\frac{1}{2}\left(\frac{|u_L|}{|u_K|}+1\right)=\cos\left[2\left(\arctan\frac{\omega_K}{\omega_0}-\arctan\frac{\omega_L}{\omega_0}\right)\right] \quad \text{(S7)}$$

Considering $\cos 2\alpha=\frac{1-\tan^2\alpha}{1+\tan^2\alpha}$ and $\tan(\alpha-\beta)=\frac{\tan\alpha-\tan\beta}{1+\tan\alpha\tan\beta}$,

$$\frac{1}{2}\left(\frac{|u_L|}{|u_K|}+1\right)=\frac{\left(\omega_0^2+\omega_K\omega_L\right)^2-\omega_0^2\left(\omega_K-\omega_L\right)^2}{\left(\omega_0^2+\omega_K\omega_L\right)^2+\omega_0^2\left(\omega_K-\omega_L\right)^2} \quad \text{(S8)}$$

For the sake of narrative convenience, in the following discussion, $u_K=|u_K|, u_L=|u_L|$.

By setting $A'=\sqrt{\frac{u_K-u_L}{3u_K+u_L}}, B'=\omega_L-\omega_K, C'=\omega_L\omega_K\sqrt{\frac{u_K-u_L}{3u_K+u_L}}$, the above equation becomes $A'\omega_0^2+B'\omega_0+C'=0$. Therefore,

$$\omega_{01,2}=\frac{\omega_K-\omega_L\pm\sqrt{\left(\omega_K-\omega_L\right)^2-4\frac{u_K-u_L}{3u_K+u_L}\omega_L\omega_K}}{2\sqrt{\frac{u_K-u_L}{3u_K+u_L}}} \quad \text{(S9)}$$

Since the base value is a positive real number, there is a constraint that $\left(\omega_K-\omega_L\right)^2-4\frac{u_K-u_L}{3u_K+u_L}\omega_L\omega_K\geq 0$. Therefore, the power system is synchronously stable when $1-\frac{4\left(\omega_K-\omega_L\right)^2}{\left(\omega_K+\omega_L\right)^2}\leq\frac{|u_L|}{|u_K|}\leq 1$.

$$1-\frac{4\left(\omega_K-\omega_L\right)^2}{\left(\omega_K+\omega_L\right)^2}=\frac{|u_L|}{|u_K|} \quad \text{(S10)}$$

is the stability boundary at the absolute velocity. When $u_K=u_L$, $\omega_K-\omega_L$ can take any value, which is exactly the left side of Eq. (1). When $u_K=u_L$, Eq. (S10) is equivalent to the right side of Eq. (1).This boundary equation is still determined by the behavior of individuals in the system and is independent of ω_0 and the network.

Proof of the Boundary Equation

$$\delta_i=2\arctan\frac{\omega_i}{\omega_0}$$

The derivation of Eq. (1) is heuristic, and is the basis for Δu and ∂u. However, to the best of the author's knowledge, this is a transformation that has not been mentioned in other studies. Eq. (1) is a stability boundary yet to be proven.

By the definition of synchronous stability, for any real number $\varepsilon>0$, a system is synchronously stable if there exists $\delta(\varepsilon)>0$ such that the system satisfies $\|\omega_K-\omega_L\|\leq\varepsilon$ when $\|\omega_{01}-\omega_{02}\|\leq\delta(\varepsilon)$. Therefore, according to the definition of a stable boundary, the $(\omega_K-\omega_L)_{\max}$

is the synchronization stable boundary when $\delta(\varepsilon)>0$ exists. The condition for the existence of $\delta(\varepsilon)$ is that both ω_{01} and ω_{02} exist.

Define $\|\omega_{01}-\omega_{02}\|=\delta(\varepsilon)=\dfrac{\sqrt{\varepsilon^2-\eta^2\omega_K\omega_L}}{\eta}$, where $\varepsilon=\|\omega_K-\omega_L\|$, $\eta=2\sqrt{\dfrac{u_K-u_L}{3u_K+u_L}}$. $\delta(\varepsilon)>0$ is required to be real numbers. If $\delta(\varepsilon)>0$ exists, it is required that $\varepsilon^2\geq\eta^2\omega_K\omega_L$. Since ε is a positive real number, $\varepsilon\geq 2\sqrt{\dfrac{u_K-u_L}{3u_K+u_L}\omega_K\omega_L}$ is obtained. Since the synchronization stability of the system is required to satisfy $\|\omega_K-\omega_L\|\leq\varepsilon$, $(\omega_K-\omega_L)_{\max}$ is taken to be the infimum of ε, i.e., $\omega_K-\omega_L=2\sqrt{\dfrac{u_K-u_L}{3u_K+u_L}\omega_K\omega_L}$. This is precisely Eq. (S10). It is equivalent to Eq. (1).

Proof of Eq.(S2)

Let $\alpha\in[0,1]$. Assume that during period αT, $\delta_i'(t)>\delta_j'(t)$ and during period $(1-\alpha)T$, $\delta_i'(t)<\delta_j'(t)$. Substituting these results into Eqs. (S2) and (S3) yields $\begin{aligned}\delta_i&=\alpha\delta_i'+(1-\alpha)\delta_j'\\ \delta_j&=\alpha\delta_j'+(1-\alpha)\delta_i'\end{aligned}$. Consequently, we have: $\delta_i-\delta_j=(2\alpha-1)(\delta_i'-\delta_j')\geq 0$.

When the generator system δ_i',δ_j' is stable, for any real number $\varepsilon>0$ satisfies $\|\delta_i'-\delta_j'\|\leq\varepsilon$, there exists $\delta(\varepsilon)>0$ satisfying the definition of stability. Since $(2\alpha-1)\varepsilon\in\{\forall\varepsilon\}$ and $(2\alpha-1)\varepsilon\leq\varepsilon$, for any real number $\varepsilon>0$ satisfies $\|\delta_i-\delta_j\|=\|(2\alpha-1)(\delta_i'-\delta_j')\|\leq\varepsilon$, $\delta(\varepsilon)>0$ exists. That is, the meta-generator system δ_i,δ_j is also stable. $\{\forall\varepsilon\}$ means the set of elements that satisfy the condition "$\forall\varepsilon$".

When the generator system is unstable, then $\alpha=1$, $\delta_i-\delta_j=\delta_i'-\delta_j'$ [refer to Figs. 1(f), S1(e), S6(c), (f) and (l)]. The meta-generator system is also unstable.

Therefore, the condition for the stability of the meta-generator system is that the generator system is stable. That is, Eq. (S2) does not change the stability discrimination of the system.

References

1. Koronovskii, A. A., Moskalenko, O. I. & Hramov, A. E. synchronization in complex networks. *Tech. Phys. Lett.* **38**, 924–927 (2012).
2. Dörfler, F., Chertkov, M. & Bullo, F. Synchronization in complex oscillator networks and smart grids. *Proc. Natl. Acad. Sci. U. S. A.* **110**, 2005–2010 (2013).
3. Wu, K., Hao, X., Liu, J., Liu, P. & Shen, F. Online Reconstruction of Complex Networks From Streaming Data. *IEEE Trans. Cybern.* **52**, 5136–5147 (2022).
4. Linyuan, L. L. & Zhou, T. Link prediction in complex networks: A survey. *Phys. A Stat. Mech. its Appl.* **390**, 1150–1170 (2011).
5. Xu, Y., Zhou, W. & Fang, J. Topology identification of the modified complex dynamical network with non-delayed and delayed coupling. *Nonlinear Dyn.* **68**, 195–205 (2012).
6. Molnar, F., Nishikawa, T. & Motter, A. E. Asymmetry underlies stability in power grids. *Nat. Commun.* **12**, 1–9 (2021).
7. Martínez, I., Messina, A. R. & Vittal, V. Normal form analysis of complex system models: A structure-preserving approach. *IEEE Trans. Power Syst.* **22**, 1908–1915 (2007).

8. Zhu, L. & Hill, D. J. Synchronization of Kuramoto Oscillators: A Regional Stability Framework. *IEEE Trans. Automat. Contr.* **65**, 5070–5082 (2020).
9. Casals, M. R. *et al.* Knowing power grids and understanding complexity science. *Int. J. Crit. Infrastructures* **11**, 4 (2015).
10. Gurrala, G., Dimitrovski, A., Pannala, S., Simunovic, S. & Starke, M. Parareal in Time for Fast Power System Dynamic Simulations. *IEEE Trans. Power Syst.* **31**, 1820–1830 (2016).
11. Gurrala, G. *et al.* Large Multi-Machine Power System Simulations Using Multi-Stage Adomian Decomposition. *IEEE Trans. Power Syst.* **32**, 3594–3606 (2017).
12. Wang, B., Fang, B., Wang, Y., Liu, H. & Liu, Y. Power System Transient Stability Assessment Based on Big Data and the Core Vector Machine. *IEEE Trans. Smart Grid* **7**, 2561–2570 (2016).
13. Yu, Y., Liu, Y., Qin, C. & Yang, T. Theory and Method of Power System Integrated Security Region Irrelevant to Operation States: An Introduction. *Engineering* **6**, 754–777 (2020).
14. Yang, P., Liu, F., Wei, W. & Wang, Z. Approaching the Transient Stability Boundary of a Power System: Theory and Applications. *IEEE Trans. Autom. Sci. Eng.* 1–12 (2022) doi:10.1109/TASE.2022.3213678.
15. Al-Ammar, E. A. & El-Kady, M. A. Application of operating security regions in power systems. *IEEE PES Transm. Distrib. Conf. Expo. Smart Solut. a Chang. World* (2010) doi:10.1109/TDC.2010.5484270.
16. Kundur, P. *et al.* Definition and classification of power system stability. *IEEE Trans. Power Syst.* **19**, 1387–1401 (2004).
17. Student Member, B. B. & Senior Member, G. A. On the nature of unstable equilibrium points in power systems. *IEEE Trans. Power Syst.* **8**, 738–745 (1993).
18. Chiang, H. D., Wu, F. F. & Varaiya, P. P. A BCU Method for Direct Analysis of Power System Transient Stability. *IEEE Trans. Power Syst.* **9**, 1194–1208 (1994).
19. Shubhanga, K. N. & Kulkarni, A. M. Application of Structure Preserving Energy Margin Sensitivity to Determime the Effectiveness of Shunt and Serles FACTS Devices. *IEEE Power Eng. Rev.* **22**, 57 (2002).
20. Bhui, P. & Senroy, N. Real-Time Prediction and Control of Transient Stability Using Transient Energy Function. *IEEE Trans. Power Syst.* **32**, 923–934 (2017).
21. Al Marhoon, H. H., Leevongwat, I. & Rastgoufard, P. A fast search algorithm for Critical Clearing Time for power systems transient stability analysis. *2014 Clemson Univ. Power Syst. Conf. PSC 2014* (2014) doi:10.1109/PSC.2014.6808093.
22. Rimorov, D., Wang, X., Kamwa, I. & Joos, G. An approach to constructing analytical energy function for synchronous generator models with subtransient dynamics. *IEEE Trans. Power Syst.* **33**, 5958–5967 (2018).
23. Motter, A. E., Myers, S. A., Anghel, M. & Nishikawa, T. Spontaneous synchrony in power-grid networks. *Nat. Phys.* **9**, 191–197 (2013).
24. Li, X., Wei, W. & Zheng, Z. Promoting synchrony of power grids by restructuring network topologies. *Chaos An Interdiscip. J. Nonlinear Sci.* **33**, 63149 (2023).
25. Kuramoto, Y. & Battogtokh, D. Coexistence of Coherence and Incoherence in Nonlocally Coupled Phase Oscillators. *Physics (College. Park. Md).* **4**, 380–385 (2002).
26. Martens, E. A., Thutupalli, S., Fourrière, A. & Hallatschek, O. Chimera states in mechanical oscillator networks. *Proc. Natl. Acad. Sci. U. S. A.* **110**, 10563–10567 (2013).
27. Panaggio, M. J. & Abrams, D. M. Chimera states: Coexistence of coherence and incoherence in networks of coupled oscillators. *Nonlinearity* **28**, R67–R87 (2015).
28. Ding, L., Gonzalez-Longatt, F. M., Wall, P. & Terzija, V. Two-step spectral clustering controlled islanding algorithm. *IEEE Trans. Power Syst.* **28**, 75–84 (2013).
29. Ajala, O., Dominguez-Garcia, A., Sauer, P. & Liberzon, D. A Second-Order Synchronous Machine Model for Multi-swing Stability Analysis. *51st North Am. Power Symp. NAPS 2019* (2019) doi:10.1109/NAPS46351.2019.9000368.
30. Alberto, L. F. C. & Bretas, N. G. Required damping to assure multiswing transient stability: the SMIB case. *Int. J. Electr. Power Energy Syst.* **22**, 179–185 (2000).
31. Pecora, L. M., Sorrentino, F., Hagerstrom, A. M., Murphy, T. E. & Roy, R. Cluster synchronization and isolated desynchronization in complex networks with symmetries. *Nat. Commun.* **5**, (2014).

32. Denker, M., Timme, M., Diesmann, M., Wolf, F. & Geisel, T. Breaking Synchrony by Heterogeneity in Complex Networks. *Phys. Rev. Lett.* **92**, 1–4 (2004).
33. Karatekin, C. Z. & Uçak, C. Sensitivity analysis based on transmission line susceptances for congestion management. *Electr. Power Syst. Res.* **78**, 1485–1493 (2008).
34. Nishikawa, T. & Motter, A. E. Symmetric States Requiring System Asymmetry. *Phys. Rev. Lett.* **117**, 114101 (2016).
35. Dörfler, F. & Bullo, F. Synchronization in complex networks of phase oscillators: A survey. *Automatica* **50**, 1539–1564 (2014).
36. Fan, H., Wang, Y. & Wang, X. Eigenvector-based analysis of cluster synchronization in general complex networks of coupled chaotic oscillators. *Front. Phys.* **18**, (2023).
37. Anderson, P. M. & Fouad, A. A. *Power System Control and Stability*. (John Wiley & Sons, 2008).
38. Pai, A. *Energy Function Analysis for Power System Stability*. (Springer Science & Business Media, 1989).
39. NIU, M., WAN, C. & XU, Z. A review on applications of heuristic optimization algorithms for optimal power flow in modern power systems. *J. Mod. Power Syst. Clean Energy* **2**, 289–297 (2014).